

DTP/96/02  
February 1996

# Constraints on gluon evolution at small $x$ <sup>1</sup>

J. Kwiecinski<sup>2</sup>, A. D. Martin and P. J. Sutton,

Department of Physics, University of Durham, Durham, DH1 3LE, England

## Abstract

The BFKL and the unified angular-ordered equations are solved to determine the gluon distribution at small  $x$ . The impact of kinematic constraints is investigated. Predictions are made for observables sensitive to the gluon at small  $x$ . In particular comparison is made with measurements at the HERA electron-proton collider of the proton structure function  $F_2(x; Q^2)$  as a function of  $\ln Q^2$ , the charm component,  $F_2^c(x; Q^2)$  and diffractive  $J=$  photoproduction.

---

<sup>1</sup>Submitted to Zeitschrift für Physik C

<sup>2</sup>On leave from Henryk Niewodniczanski Institute of Nuclear Physics, 31-342 Krakow, Poland.

## 1. Introduction

Understanding the small  $x$  behaviour of the gluon density is one of the most challenging problems of perturbative QCD. It has become topical with the commissioning of the electron-proton collider HERA at DESY. Indeed experiments at HERA are probing the gluon density in the region  $x < 10^{-3}$  by observation of the behaviour of the proton structure function<sup>3</sup>  $F_2$  as a function of  $\ln Q^2$  and by the measurements of diffractive  $J/\psi$  photoproduction, dijet production etc. [1, 2, 3].

First we recall that for moderate values of  $x$ , say  $x > 0.05$ , observable quantities such as  $F_2(x; Q^2)$  are determined in perturbative QCD by the mass factorization theorem in which the collinear logarithmic singularities, that arise from gluon emissions in the partonic subprocesses, are absorbed into universal parton densities. The absorption of the collinear singularities make the densities run with a  $Q^2$  dependence determined by the Altarelli-Parisi (GLAP) evolution equations, although the absolute values of the densities are not calculable in perturbative QCD but have to be input at some scale, say  $Q_0^2$ . In fact Altarelli-Parisi evolution resums the leading  $\ln(Q^2/Q_0^2)$  contributions where, in a physical gauge, the  $\ln^n(Q^2/Q_0^2)$  contribution is associated with a space-like chain of  $n$  gluon emissions in which the successive gluon transverse momenta are strongly ordered along the chain, that is  $q_{T1}^2 \gg \dots \gg q_{Tn}^2 \sim Q^2$ . The coefficient (splitting) functions and anomalous dimensions of Altarelli-Parisi evolution have been calculated to next-to-leading order. This corresponds to the situation in which a pair of gluons are emitted without strong  $q_T$  ordering (and iterations of this configuration). Then the contributions contain a power of  $\ln(Q^2/Q_0^2)$ .

At sufficiently high electron-proton c.m. energy,  $\sqrt{s}$ , we encounter a second large variable,  $1-x = s/Q^2$ , and we must resum the leading  $\ln(1-x)$  contributions. In this regime the dominant parton is the gluon and the key ingredients to calculate hard scattering observables are the  $k_T$ -factorization theorem and the BFKL equation for the gluon distribution  $F(x; k_T^2)$  unintegrated over its transverse momentum  $k_T$  [4, 5]. The BFKL equation, which sums the leading  $\ln(1-x)$  contributions, may be written in the form [6, 7]

$$F(x; k_T^2) = F^{(0)}(x; k_T^2) + \frac{1}{s} \int_x^1 \frac{dz}{z} \int \frac{d^2 q_T}{q_T^2} F\left(\frac{x}{z}; k_T + q_T\right) (k_T^2 - q_T^2) F\left(\frac{x}{z}; k_T^2\right) \quad (1)$$

with  $\frac{1}{s} = 3/s$ , and where  $F^{(0)}$  is the non-perturbative driving term of the equation. To gain insight into the equation we refer to Fig. 1 which shows the basic unit that, on iterating (1), leads to a chain of sequential gluon emissions. These real emissions come from the first term under the integral, where  $k_T + q_T = k_T^0$  of Fig. 1. The second term corresponds to the virtual contributions which arise from gluon loops along the chain. The real and virtual contributions

<sup>3</sup>In deep inelastic scattering we do not probe the gluon directly, but instead via the process  $g \rightarrow q\bar{q}$ . The longitudinal fraction  $x$  of the proton's momentum that is carried by the gluon is therefore sampled over an interval bounded below by the Bjorken  $x$  variable  $x_b = Q^2/2px$ , where as usual  $p$  and  $q$  are the four momenta of the incoming proton and virtual photon respectively and  $Q^2 = -q^2$ . We omit the subscript  $b$  since the distinction between  $x$  (of the gluon distribution) and  $x_b$  in  $F_2(x_b; Q^2)$  is evident.

cancel as  $q_T \rightarrow 0$  to ensure that there is no singularity in (1). The strong ordering in  $q_T$  is now no longer applicable and instead we have a "random walk" or diffusion in  $\ln q_T^2$  as we proceed along the chain to gluons with smaller and smaller values of  $x$ . The enlarged  $q_T$  phase space leads to a  $x^{-1}$  type growth of  $F$  as  $x \rightarrow 0$ . In fact, since the kernel of the BFKL equation is scale invariant, the solution can be found by Mellin transform techniques and given analytically for  $x \rightarrow 0$  (for fixed coupling  $g_s$ ). In particular we have the famous result, obtained in the original BFKL papers [6], that

$$F = g_s^{-4} \ln 2 \quad (2)$$

corresponding to the maximum of a continuous spectrum of eigenvalues of the kernel of the (Mellin-transformed) BFKL equation.

The BFKL equation sums the leading order  $g_s \ln(1/x)$  contributions. The next-to-leading terms are not yet known. However, there is one kinematical constraint which should be implemented, namely [7, 8]

$$k_T^2 > z q_T^2 : \quad (3)$$

The constraint<sup>4</sup> arises since, in the small  $z$  regime where the BFKL equation is valid, we require that the virtuality of the exchanged gluons arises mainly from the transverse, rather than the longitudinal, components of their momentum; that is

$$k^0 f^2 \ll k_T^0 f^2 : \quad (4)$$

There are also constraints from energy-momentum conservation [9]. For example, for the gluon of transverse momentum  $k_T^0$  forming one of the links of the BFKL chain we require  $(q + k^0)^2 > 0$ , where  $q$  is the four momentum of the deep inelastic photon probe. That is

$$k_T^0 < \frac{Q^2}{x} \quad W^2 \quad (5)$$

at small Bjorken  $x$ . However (3) gives an implicit bound on  $k_T^0$  which is usually much more restrictive than (5). This can be seen by considering a given value of  $k_T^2$ : Then a high value of  $q_T^2$  implies an equally high value of  $k_T^0$  and (3) becomes

$$k_T^0 < \frac{k_T^2}{z} : \quad (6)$$

Since  $z > x$ , this bound is tighter than (5) except for low values of  $Q^2$  which are much less than  $k_T^2$ . This is fortunate because it is possible to study the effects of imposing (3) on the solution of the BFKL equation. Indeed, the introduction of the upper limit of integration,  $q_T^2 < k_T^2 = z$ , preserves the scale invariance of the BFKL equation and therefore allows the Mellin transform technique to be used to find the modified form of the solution as  $x \rightarrow 0$ , see Section 2. The modifications enter at next-to-leading order and above. They are found to reduce the exponent

---

<sup>4</sup>Throughout we call this a kinematic constraint although its origin is partly dynamical. We sketch the derivation of (3) in Section 3.

of the  $x$  behaviour from the BFKL value given in (2). Besides finding the analytic solution, we also solve the BFKL equation numerically and present results for the effective value of  $s$  at non-zero values of  $x$  so that we can study how the asymptotic ( $x \rightarrow 0$ ) analytic result is approached.

If  $s$  is allowed to run then the integrand in the BFKL equation is weighted more to the infrared end, and the effects of the kinematic constraint (3) will become weaker. We investigate the effect in terms of the unified CCFM evolution equation [7, 10, 11], which reduces to the BFKL equation in the small  $x$  limit. The CCFM equation is based on the coherent radiation of gluons, which leads to an angular ordering in their emissions [12]. The gluon distribution, which satisfies the CCFM equation, depends on an additional scale that is required to specify the maximum angle possible for gluon emission, which is given essentially by the scale of the probe. The gluon distribution therefore becomes a function of three variables  $F(x; k_T^2; Q^2)$ . In particular, angular ordering introduces a constraint

$$q_T^2 < \frac{Q^2}{z^2} (1 - z)^2 \quad (7)$$

into the integrand of the equation for the gluon. At small  $z$ , this angular-ordering constraint  $q_T^2 < Q^2 = z^2$  appears much weaker than the kinematic constraint  $q_T^2 < k_T^2 = z$  of (3). Clearly for  $Q^2 > k_T^2$  we would expect no effect from angular ordering and the gluon distribution would become independent of  $Q^2$ . In Section 3 we solve the CCFM equation numerically, with and without imposing the kinematic constraint (3), so as to study these effects.

In Section 4 we use the results for the unintegrated gluon distribution, together with the  $k_T$ -factorization theorem, to study the effect of the kinematic constraint on observable small  $x$  processes. In particular we make predictions for the behaviour of  $F_2(x; Q^2)$  as a function of  $\ln Q^2$  at small  $x$ , for its charm component  $F_2^c(x; Q^2)$ , and for high energy diffractive  $J=$  photoproduction. Data are available for these three processes, all of which are sensitive to the gluon at small  $x$  [1, 2, 3]. We present our conclusions in Section 5.

## 2. Constraints on the gluon from the BFKL equation with fixed $s$

In this section we investigate the effect of imposing the kinematic constraint  $q_T^2 < k_T^2 = z$  on the solution of the BFKL equation, (1). In particular we wish to solve the equation for the unintegrated gluon distribution which incorporates the constraint,

$$F(x; k_T^2) = F^{(0)}(x; k_T^2) + \frac{1}{s} \int_0^1 \frac{dz}{z} \int \frac{d^2 q_T}{q_T^2} \frac{k_T^2}{q_T^2} \int \frac{d^2 k_T}{k_T^2} F\left(\frac{x}{z}; k_T^2 + q_T^2\right) (k_T^2 - q_T^2) F\left(\frac{x}{z}; k_T^2\right); \quad (8)$$

and to determine the value of the exponent of the  $x$  behaviour of the solution. The solution can most easily be obtained by rewriting the equation in terms of the gluon distribution in momentum space

$$\bar{F}(\ell; k_T^2) = \int_0^1 dx x^{\ell-1} F(x; k_T^2); \quad (9)$$

Then the BFKL equation becomes

$$\begin{aligned} \overline{F}(\omega; k_T^2) = & \overline{F}^{(0)}(\omega; k_T^2) + \frac{1}{s} \int_0^1 \frac{d^2 q_T}{q_T^2} \int_0^{1-\omega} \frac{dz}{z} z^{\omega-1} \frac{k_T^2}{q_T^2} z^{\omega} \overline{F}(\omega; k_T^2 + q_T^2) \\ & - \frac{1}{\omega} (k_T^2 - q_T^2) \overline{F}(\omega; k_T^2) \end{aligned} \quad (10)$$

where the first function imposes the kinematic constraint on the real emissions. As usual we solve the equation by taking the Mellin transform, and introduce the variable conjugate to  $k_T^2$

$$\overline{F}(\omega; k_T^2) = \frac{1}{2-i} \int_{c-i\infty}^{c+i\infty} d(k_T^2) F(\omega; k_T^2) \quad (11)$$

then the BFKL equation reduces to the algebraic relation

$$F(\omega; k_T^2) = F^{(0)}(\omega; k_T^2) + \frac{1}{s} K(\omega; k_T^2) F(\omega; k_T^2) \quad (12)$$

where the kernel

$$K(\omega; k_T^2) = \int_0^1 \frac{d^2 q_T}{q_T^2} \int_0^{1-\omega} \frac{dz}{z} z^{\omega-1} \frac{k_T^2}{q_T^2} z^{\omega} \overline{F}(\omega; k_T^2 + q_T^2) - \frac{1}{\omega} (k_T^2 - q_T^2) \overline{F}(\omega; k_T^2) \quad (13)$$

The expression arising from the first term in (10), up to a factor of  $1/s$ . The kernel is scale invariant, as becomes evident once we make the substitution  $q_T^2 = k_T^2 u$ . Then (13) becomes

$$\begin{aligned} K(\omega; k_T^2) = & \int_0^1 \frac{d^2 q_T}{q_T^2} \int_0^{1-\omega} \frac{du}{u} u^{\omega-1} (1 + 2\sqrt{u} \cos \theta + u) (1 + u)^{-\omega-1} \\ = & \int_0^1 \frac{du}{u} F(\omega; k_T^2; 1; u) (1 + u)^{-\omega-1} \end{aligned} \quad (14)$$

where  $F(\omega; k_T^2; 1; u)$  is the hypergeometric function, and where the  $u$  term arises from the integration over the interval  $1 < u < 1$  when we substitute  $u = 1/u$ .

The solution of the BFKL equation for the double Mellin transform  $F(\omega; k_T^2)$  has the usual form

$$F(\omega; k_T^2) = \frac{F^{(0)}(\omega; k_T^2)}{1 - \frac{1}{s} K(\omega; k_T^2)} \quad (15)$$

except that now due to presence of the  $q_T^2 < k_T^2 = z$  cut,  $K$  depends on  $\omega$ , as well as  $k_T^2$ . Inverting the moments in the standard way we find that the unintegrated distribution is given by

$$F(x; k_T^2) = \frac{1}{2-i} \int_{c-i\infty}^{c+i\infty} d(k_T^2) R(\omega) x^{-\omega} \quad (16)$$

where we have performed the  $\omega$  integration, and picked up the "leading" pole of  $F(\omega; k_T^2)$  at  $\omega = \omega(k_T^2)$ , with residue  $R(\omega)$ . From (15) we see that the pole position  $\omega(k_T^2)$  is a solution of the equation

$$1 - \frac{1}{s} K(\omega(k_T^2); k_T^2) = 0 \quad (17)$$

The exponent of the  $x$  behaviour, or in other words the pole position  $\Gamma(\gamma)$  which determines the leading behaviour of (16) as  $x \rightarrow 0$ , is the maximum value of  $\Gamma(\gamma)$  as  $\gamma$  varies along the contour  $c - i1$  to  $c + i1$  where  $c$  lies in the interval  $(1/2; 1)$ . The value  $\Gamma(\gamma)$  is found from

$$\frac{dK(\gamma; \gamma)}{d\gamma} = 0 \quad (18)$$

which occurs at the saddle point  $\gamma = \gamma_s = c$ . The resulting values for the intercept

$$\gamma = \Gamma(\gamma) \quad (19)$$

are shown as a function of  $\gamma_s$  by the continuous curve in Fig 2.

The curve is to be compared with the leading-order intercept, shown as a dashed line, which is obtained from the BFKL equation without the kinematic constraint imposed. In this case we have  $\gamma = 0$  in  $K(\gamma; \gamma)$  in (12) and so  $K$  is a function of  $\gamma$  alone

$$K(\gamma = 0; \gamma) = 2(1 - \gamma) \ln(1 + \gamma) \quad (20)$$

where  $\ln$  is the logarithmic derivative of the Euler function:  $\psi(z) = \frac{d}{dz} \ln \Gamma(z)$ . Along the contour of integration in (16) the pole position  $\gamma = \gamma_s K$  reaches its maximum value at the "saddle" point  $\gamma = c = \frac{1}{2}$ , and so we recover the familiar leading-order BFKL intercept

$$\gamma = \gamma_s K(\gamma = 0; \gamma = \frac{1}{2}) = \gamma_s 4 \ln 2 \quad (21)$$

It is easy to see that the imposition of the kinematic constraint in the BFKL equation introduces higher-order corrections to the value of the intercept. For instance we note that the pole in (15) is a solution of

$$\gamma = \gamma_s K(\gamma = 0; \gamma) + \gamma_s \gamma \frac{\partial K(\gamma; \gamma)}{\partial \gamma} \bigg|_{\gamma=0} + \dots \quad (22)$$

If we were to keep only the next-to-leading term in our determination of the intercept, then we would have

$$\gamma = \gamma_s 4 \ln 2 (1 - 4 \ln 5 \gamma_s);$$

which is shown by the dotted curve denoted by (c) in Fig. 2. The importance of the higher-order corrections is evident, even for values of  $\gamma_s = 3 \gamma_s = 0.1$ .

The above analytic procedure yields the "asymptotic" or leading  $x$  behaviour of the gluon distribution  $F(x; k_T^2)$  as  $x \rightarrow 0$ . We may solve the modified BFKL equation numerically to see how the asymptotic value of the intercept is approached as  $x$  decreases, for different values of  $k_T^2$ . To be precise we solve (8) numerically using for the driving term  $F^{(0)}(x; k_T^2)$  a conventional distribution of the form  $3(1-x)^5 N \exp(-k_T^2/k_0^2)$  with  $k_0 = 1 \text{ GeV}$ . In Fig. 3 we show the effective slope  $\gamma_e$ , obtained from the solution  $F(x; k_T^2)$  via

$$\gamma_e = \frac{\partial \ln F}{\partial \ln(1/x)}; \quad (23)$$

as a function of  $x$  for different values of  $k_T^2$ , for a fixed  $\bar{s} = 0.2$ . We see that the approach to the asymptotic ( $x \rightarrow 0$ ) value,  $\bar{s} = 0.35$ , depends on the value of  $k_T^2$ . Since  $\bar{s}$  is the leading singularity we would expect an approach from below. However, for large  $k_T^2$  the  $x$  dependence of the BFKL diffusion pattern,

$$\exp @ \quad A \frac{\ln^2(k_T^2 = \bar{k}_T^2) A}{\ln(1-x)} ;$$

overrides this behaviour and causes  $\bar{s}$  to approach the asymptotic value from above. Here  $\bar{k}_T^2$  is associated with the non-perturbative input distribution.

## 2.1 Kinematic constraint in the folded form of the BFKL equation

In Section 3 we study the effect of the kinematic constraint in the more realistic case when  $\bar{s}$  is allowed to run. There we solve the evolution equation in "folded" form. That is the form in which all the virtual corrections and all the unresolved real gluon emissions are resummed. Unresolved emissions are those with  $q_F^2 < \bar{s}^2$ , where  $\bar{s}^2$  specifies the resolution. Imposing the kinematic constraint  $q_F^2 < k_T^2 = z$  on the folded BFKL equation is a little more involved than it was in the "unfolded" form (8) in which the real and virtual terms appear on an equal footing, that is to the same order in  $\bar{s}$ . To see this we first rewrite the unfolded BFKL equation, (10), in the form

$$\begin{aligned} \bar{F}(!; k_T^2) = & \bar{F}^{(0)}(!; k_T^2) + \frac{\bar{s}^z}{!} \frac{d^2 q_F}{q_F^2} (k_T^2 - q_F^2) \bar{F}(!; k_T + q_F) - \bar{F}(!; k_T^2) \\ & + \frac{\bar{s}^z}{!} \frac{d^2 q_F}{q_F^2} (q_T^2 - k_T^2) \frac{k_T^2}{q_F^2} \bar{F}(!; k_T + q_F) \end{aligned} \quad (24)$$

where we have simply divided the  $q_F$  integration according to whether  $q_F^2$  is less or greater than  $k_T^2$ , and carried out the  $z$  integrations. The kinematic constraint is responsible for the factor  $(\cdot)^!$  in the second integral. Now we divide the first integral according to whether  $q_F^2 < \bar{s}^2$  or  $q_F^2 > \bar{s}^2$  so that we can resum all the virtual and unresolved real terms. Providing  $\bar{s}^2$  is not too large, we can evaluate the  $q_F^2 < \bar{s}^2$  part explicitly:

$$\begin{aligned} \frac{\bar{s}^z}{!} \frac{d^2 q_F}{q_F^2} \bar{F}(!; k_T + q_F) &= \frac{\bar{s}^z}{!} \bar{F}(!; k_T^2) \frac{d^2 q_F}{q_F^2} + O\left(\frac{\bar{s}^2}{k_T^2}\right), \quad \frac{\bar{s}^z}{!} \bar{F}(!; k_T^2) \\ &= \frac{\bar{s}^z}{!} \bar{F}(!; k_T^2) \frac{d^2 q_F}{q_F^2} + O\left(\frac{\bar{s}^2}{k_T^2}\right), \end{aligned} \quad (25)$$

where

$$\bar{s}^z = \bar{s} \ln(k_T^2 = \bar{s}^2): \quad (26)$$

The result (25) is the residual virtual correction to  $\bar{F}(!; k_T^2)$  which remains after the cancellation of the unresolved real and virtual singularities. Using (25), we see that then (24) becomes

$$\begin{aligned} \bar{F}(!; k_T^2) = & \hat{F}^{(0)}(!; k_T^2) + \frac{\bar{s}^z}{! + \bar{s}} \frac{d^2 q_F}{q_F^2} (k_T^2 - q_F^2) (q_T^2 - \bar{s}^2) \bar{F}(!; k_T + q_F) \\ & + \frac{\bar{s}^z}{! + \bar{s}} \frac{d^2 q_F}{q_F^2} \frac{k_T^2}{q_F^2} (q_T^2 - k_T^2) (q_T^2 - \bar{s}^2) \bar{F}(!; k_T + q_F); \end{aligned} \quad (27)$$

where  $\hat{F}^{(0)} = \hat{F}^{(0)} = \hat{F}^{(0)} = (\hat{F} + \hat{T})$ . We invert the moments and transform back to  $x$  space, and find

$$F(x; k_T^2) = \hat{F}^{(0)}(x; k_T^2) + \int_0^1 \frac{dz}{z} \frac{d^2 q_T}{q_T^2} \frac{k_T^2}{q_T^2} z (q_T^2 - z^2) \tilde{R}(z; k_T^2; q_T^2; z^2) F\left(\frac{x}{z}; \vec{k}_T + \vec{q}_T; q^2\right) \quad (28)$$

where  $\tilde{R}$ , often called the non-Sudakov form factor, is given by

$$\tilde{R}(z; k_T^2; q_T^2; z^2) = \exp \left( - \int_0^1 \frac{dz^0}{z^0} \frac{k_T^2}{q_T^2} z^0 \int \frac{d\vec{q}_T^0}{q_T^{02}} (k_T^2 - \vec{q}_T^0) (q_T^{02} - z^2) \right) \\ = \begin{cases} \approx z^T & \text{if } q_T^2 < k_T^2 \\ \approx (z q_T^2 = k_T^2)^T & \text{if } q_T^2 > k_T^2; \end{cases} \quad (29)$$

where  $T$  is given by (26). The form factor screens the  $1/z$  singularity in (28).

We see that the inclusion of the kinematic constraint  $q_T^2 < k_T^2 = z$  in the real gluon emission part of the unfolded BFKL equation, (8), has the additional effect of modifying the non-Sudakov form factor in the folded equation (28). The modification occurs for  $q_T^2 > k_T^2$  and makes the form factor larger, but always, of course, satisfying  $\tilde{R} < 1$ .

### 3. Constraints on the gluon from the CCFM equation

The BFKL equation, which resums the  $\sim \ln(1-x)$  contributions, is applicable at small  $x$  and moderate  $Q^2$ , whereas at larger  $x$  and large  $(Q^2 = Q_0^2)$  Altarelli-Parisi (GLAP) evolution, which resums the  $\sim \ln(Q^2 = Q_0^2)$  terms, is appropriate. A theoretical framework which gives a unified treatment throughout the  $x; Q^2$  region has been formulated by Ciafaloni, Catani, Fiorani and Marchesini [10]. The CCFM approach is based on the coherent radiation of gluons which implies angular ordering of the gluon emissions along the chain. The CCFM equation embodies both the BFKL and GLAP equations in the appropriate kinematic regimes. In the small  $x$  region the CCFM equation may be approximated by [11]

$$F(x; k_T^2; Q^2) = \hat{F}^{(0)}(x; k_T^2; Q^2) + \int_0^1 \frac{dz}{z} \frac{d^2 q}{q^2} (Q^2 - zq^2) \tilde{R}(z; k_T^2; q_T^2) F\left(\frac{x}{z}; \vec{k}_T + \vec{q}_T; q^2\right) \quad (30)$$

where it is convenient to impose the angular ordering in terms of rescaled transverse momenta

$$q = \frac{q_T}{1-z}; \quad (31)$$

The angular-ordering constraint then becomes  $q < Q = z$ . Here the non-Sudakov form factor  $R$  is given by

$$R(z; k_T^2; q_T^2) = \exp \left[ -s(k_T^2) \int_z^1 \frac{dz^0}{z^0} \frac{dq_T^2}{q_T^2} (k_T^2, q_T^2) (q^0, zq) \right] \quad (32)$$

Finally, note that we have allowed  $s$  to run in (30). The solutions  $F(x; k_T^2; Q^2)$  of this equation were studied in ref. [11]. As in ref. [11] we restrict the transverse momenta of the gluons along the chain to be above  $1 \text{ GeV}^2$ . As we shall see it turns out that this physically reasonable choice of infrared cut-off gives a satisfactory normalization of all the observables sensitive to the small  $x$  behaviour of the gluon distribution,  $F$ , with the exception of  $F_2^c$  at low  $Q^2$ .

The novel feature of the CCFM, as compared to the BFKL equation, is that the solution is dependent on  $Q^2$ . The origin of the dependence comes entirely from angular ordering,  $q < Q = z$ . In the BFKL leading  $\ln(1/x)$  limit  $F$  becomes independent of  $Q^2$  and indeed the CCFM solutions exhibit this behaviour for large  $Q^2$ . However, for small  $Q^2$  non-leading  $\ln(1/x)$  effects become important via the angular ordering constraint and  $F$  decreases with decreasing  $Q^2$  [11].

Here we study the impact of the kinematic constraint  $q_T^2 < k_T^2 = z$ . To be precise the constraint is actually

$$q_T^2 < (1 - z) k_T^2 = z: \quad (33)$$

We sketch the derivation. The key observation is that the virtuality  $k^2$  of a gluon along the chain should arise mainly from the transverse, rather than the longitudinal, components of the momentum for the small  $x$  approximation to be valid. Now in terms of the light-cone variables  $k = k_0 - k_3$

$$k^2 = k^+ k^- - k_T^2 \quad (34)$$

so we require

$$k_T^2 > k^+ k^-: \quad (35)$$

From Fig. 1 we see that

$$k^- = k^0 - q^-, \quad q^- = q_T^2/q^+; \quad (36)$$

where the last equality follows from the on-shell condition for the emitted gluon<sup>5</sup>. Thus

$$k^+ k^- = \frac{k^+}{q^+} q_T^2 = \frac{k^+}{k^{0+} - k^+} q_T^2 = \frac{z}{1 - z} q_T^2: \quad (37)$$

The kinematic constraint (33) then follows directly from (37) and (35).

---

<sup>5</sup>In (36) and (37)  $q^-$  are the light-cone components of the 4-momentum of the emitted gluon, whereas elsewhere in this section  $q$  denotes the rescaled transverse momentum defined by (31).

Here we wish to compare the gluon distribution  $F(x; k_T^2; Q^2)$  obtained by solving (30), with the solution obtained if the kinematic constraint (33) is imposed. That is we study the modification of the solution caused by incorporating

$$\frac{k_T^2}{(1-z)Q^2} \leq z \quad \text{and} \quad \frac{(1-z)k_T^2}{Q^2} \leq z^0 \quad (38)$$

in (30) and (32) respectively, just as the corresponding functions were included in (28) and (29). In the small  $z$ , large  $Q^2$  regime the kinematic constraint  $Q^2 < (1-z)k_T^2 = z$  is a stronger limitation than the angular ordering constraint  $Q^2 < Q^2 = z^2$ , and we anticipate that the CCFM solution  $F(x; k_T^2; Q^2)$  will become independent of  $Q^2$ . In other words in this limit the kinematic constraint automatically embodies the angular ordering constraint [8] and since the former is independent of  $Q^2$  the unintegrated gluon distribution  $F$  does not depend on this variable either. However, as  $Q^2$  decreases below  $k_T^2$  the angular ordering constraint becomes stronger and  $F$  begins to decrease. We illustrate the effect in Fig. 4 which shows  $F$  versus  $Q^2$  at different values of  $x$  for  $k_T^2 = 10 \text{ GeV}^2$ . Here we have calculated  $F$  by numerically solving the CCFM equation (30) as described in ref. [11], and then repeated the calculation with the kinematic constraints (38) incorporated. We also use these solutions to show in Fig. 5 the effective exponent  $\gamma_e$  of the integrated gluon distribution

$$\gamma_e = \frac{\partial \ln(xg)}{\partial \ln(1-x)} \quad \text{with} \quad xg(x; Q^2) = \int_0^z Q^2 F dk_T^2 \quad (39)$$

as a function of  $x$  for fixed values of  $Q^2$ . The gluon distributions are generated from a flat input ( $F^{(0)} = \text{constant}$  as  $x \rightarrow 0$ ), and so the rapid rise with decreasing  $x$  ( $xg \sim x^{-e}$ ) is generated by perturbative QCD resummation effects via the CCFM equation. As for the BFKL equation with fixed  $s$ , we notice from Fig. 5 that for the CCFM equation  $\gamma_e$  becomes smaller (by about 0.1) on imposing the kinematic constraint.

## 4. Impact on observables

Predictions for observables at small  $x$  are driven by the behaviour of the gluon distribution, since the gluon is by far the dominant parton in this regime. Here we study three quantities, which are being measured at HERA, that are especially sensitive to the gluon distribution at small  $x$ ; namely  $\partial F_2 / \partial \log Q^2$ , the charm component of  $F_2$  and high energy diffractive  $J = \text{photoproduction}$ . The first two observables are linearly dependent on the gluon density, whereas the third has a quadratic dependence which considerably increases its sensitivity to the gluon.

In deep inelastic scattering the virtual photon couples to the gluon via the  $g \rightarrow q\bar{q}$  transition. We therefore calculate the structure function  $F_2$  from the unintegrated gluon distribution  $F$  using the  $k_T$ -factorization theorem

$$F_2(x; Q^2) = \int_0^x \int_0^z dk_T^2 \int_x^z \frac{dx^0}{x^0} d^2 F(x^0; k_T^2; -^2) F_q^{\text{box}} \left( \frac{x}{x^0}; \tilde{\gamma}_T; k_T; Q^2; m_q \right) + F_2^S \quad (40)$$

where  $F_q^{\text{box}}$  includes both the quark "box" and "crossed box" contributions which originate from virtual photon-virtual gluon  $q\bar{q}$  production, that is from  $g \rightarrow q\bar{q}$ . The convolution is sketched in Fig. 6. For the u;d and s quark contributions we take the quark mass  $m_q = 0$ , while for the charm component we take  $m_c = 1.5 \text{ GeV}$ . The explicit expressions for  $F_q^{\text{box}}$  including quark mass effects can be found<sup>6</sup> in ref. [13]; the argument of  $s$  in  $F_q^{\text{box}}$  is taken to be  $(\frac{z}{T} + m_0^2)$  where  $m_0^2 = 1 \text{ GeV}^2$  for u;d;s quarks and  $m_0^2 = m_c^2$  for the c quark. The results are not very sensitive to variations of  $m_0$  about these values.

The background contribution  $F_2^S \sim F_2(x; Q^2)$  at large  $x$ , but is a slowly varying function of  $x$  and  $Q^2$  at small  $x$ . For example we extrapolate below  $x = 0.1$  using the soft Pomeron  $x^{0.08}$  behaviour. However, predictions for the slope,  $\partial F_2 / \partial \ln Q^2$  are particularly insensitive to any ambiguities due to  $F_2^S$ . The small  $x$  approximation of the CCFM equation, (30), that we have used amounts to setting the Sudakov form factor  $S = 1$  and to approximating the gluon-gluon splitting function by its singular term as  $z \rightarrow 0$ , that is  $P_{gg} \sim 6/z$ .  $S$  represents the virtual corrections which cancel the singularities at  $z = 1$ . To make a realistic comparison with data, we allow for the remaining finite terms in  $P_{gg}$  by multiplying the solution  $F(x; k_T^2; Q^2)$  by the factor

$$\exp \left[ \frac{33 + 2n_f}{36} \ln^2 Q^2 - s(q^2) \frac{dq^2}{q^2} \right]$$

where the number of active flavours  $n_f = 4$ . At large  $x$  ( $x > 0.1$ ) and small  $Q^2$  ( $Q^2 < 20 \text{ GeV}^2$ ) the CCFM solutions, with and without the kinematic constraint imposed, are found to agree with each other, and also with the solution obtained from the double-leading-logarithm (DLL) approximation of (30) in which we replace  $(Q - zq)$  by  $(Q - q)$  and set  $R = 1$ . However, at larger  $Q^2$  (beyond the range of the data that we consider here) some care is needed. The kinematic constraint is only applicable in the small  $x$  region and so the normalisation of the gluon is suspect at large  $x$ , particularly for large  $Q^2$ . We therefore renormalise the solution of the CCFM equation with the kinematic constraint imposed so as to agree for  $x > 0.1$  with the unmodified solution and its DLL approximation. In this way we allow for the small  $x$  approximation of the equation. The renormalisation only affects the solution for  $Q^2 > 20 \text{ GeV}^2$ .

In Fig. 7 we show the predictions for  $F_2(x; Q^2)$  at small  $x$  together with the latest HERA measurements. Including the kinematic constraint (33) in the CCFM equation for the gluon  $F(x; k_T^2; Q^2)$  has the effect of taking us from the dashed to the continuous curves in Fig. 7. The relevant comparison is the slope ( $\partial F_2 / \partial \ln Q^2$ ) of the curves which is proportional to the gluon distribution. With the present experimental errors the comparison is inconclusive, but it is evident that, as the statistical and systematic errors are reduced, future measurements of  $\partial F_2 / \partial \ln Q^2$  will give insight into the properties of the gluon distribution  $F(x; k_T^2; Q^2)$ .

Recently the charm component of  $F_2$  has been measured [14] at HERA in the small  $x$  region. These measurements of  $F_2^c(x; Q^2)$  are shown in Fig. 8, together with earlier EMC values [15] at larger  $x$ . We compare these data with the charm component  $F_2^c$  determined from

<sup>6</sup>There is a typographical error in the expression for  $x^0$  below eq.(19) in ref. [13]; the factor  $(1 - x)$  should be in the denominator.

the unintegrated gluon distribution,  $F$ , using the  $c$  quark contribution to the  $k_T$ -factorization formula (40). We show the values obtained by taking the mass of the charm quark to be  $m_c = 1.4$  and  $1.7$  GeV. We also show predictions based on GRV [16] and MRS partons [17]. The first of these two is obtained from  $g \rightarrow c\bar{c}$  at NLO [18] using massive charm quarks and the integrated (GRV) gluon distribution. In the MRS analyses [17, 19] the charm quark is treated as a parton. The charm distribution is assumed to be zero for  $Q^2 < m_c^2$ , while above this threshold ( $Q^2 > m_c^2$ ) it is evolved assuming that  $m_c = 0$ . The value  $m_c^2 = 2.7 \text{ GeV}^2$  is determined by fitting to the EMC data [15] for  $F_2^c$ . Although the H1 small  $x$  data are preliminary, it is clear that an improved measurement of  $F_2^c$  will be valuable. At present there are indications that our  $k_T$ -factorization approach underestimates the H1 data at the lower  $Q^2$  values; in fact the imposition of the kinematic constraint worsens our previous description of these data [20].

The third observable process that we study is high energy diffractive  $J/\psi$  photoproduction,  $p \rightarrow J/\psi + p$ . It offers a sensitive probe of the gluon at small  $x$  [21, 22]. The amplitude can be factored into the product of the  $\gamma \rightarrow c\bar{c}$  transition, the scattering of the  $c\bar{c}$  quark pair on the proton via (colourless) two-gluon exchange, and finally the formation of the  $J/\psi$  from the outgoing  $c\bar{c}$  pair. The crucial observation is that at high energy the scattering on the proton occurs over a much shorter timescale than the  $\gamma \rightarrow c\bar{c}$  fluctuation or the  $J/\psi$  formation times.

Since diffractive  $J/\psi$  photoproduction is essentially an elastic process, the cross section is dependent on the square of the unintegrated gluon distribution,  $F(x; k_T^2; Q^2)$ . The relevant values of  $x$  and  $Q^2$  are  $x = M^2/W^2$  and  $Q^2 = M^2 = 4$ , where  $M$  is the mass of the  $J/\psi$  meson and  $W$  is the  $p$  centre-of-mass energy. The cross section is given by [23]

$$\begin{aligned} \left( \frac{d\sigma}{dt} \right)_{p \rightarrow J/\psi + p} &= \frac{1}{b} \frac{d}{dt} \left( \frac{d\sigma}{dt} \right)_{p \rightarrow J/\psi + p} \\ &= \frac{3M^3}{3b} \frac{1}{s} \frac{1}{Q^2} \frac{1}{e^2} \frac{1}{k_T^2} \frac{1}{M^2} \frac{1}{M^2 + 4k_T^2} F(x; k_T^2; Q^2)^2 \end{aligned} \quad (41)$$

where  $\frac{1}{e^2}$  is the leptonic width describing the  $J/\psi \rightarrow e^+e^-$  decay,  $\frac{1}{s}$  is the QED coupling, and  $b$  is the slope parameter of the differential cross section,  $d\sigma/dt = A \exp(-b|t|)$ . We take the experimental value  $b = 4.5 \text{ GeV}^{-2}$ . We include the effects of  $c\bar{c}$  rescattering and the small contribution of the real part of the amplitude as described in ref. [23]. It was noted in ref. [23] that the effects of Fermi motion of the  $c$  and  $\bar{c}$  quarks in the  $J/\psi$  lead to a sizeable ( $\sim 30\%$ ) uncertainty in the normalization of the perturbative QCD prediction of the photoproduction cross section, but that the "shape" of the  $W$  (or  $x$ ) dependence is unaffected.

The predictions for diffractive  $J/\psi$  photoproduction are compared with recent HERA data in Fig. 9. At present the data extend up to energy  $W \sim 140 \text{ GeV}$ , that is down to  $x \sim 5 \cdot 10^{-4}$ . The prediction in the absence of the kinematic constraint (the dashed curve) implies that the gluon increases too fast with decreasing  $x$ . On the other hand if the kinematic constraint is incorporated in the CCFM equation, then the continuous curve is obtained and the description is improved.

For completeness we also show in Fig. 9 the description of the  $J=$  data calculated from two recent sets of partons (GRV [16] and MRSA<sup>0</sup> [17]) as described in ref. [23]. Neither parton set incorporates  $\ln(1=x)$  resummation effects. The  $J=$  data appear to favour the phenomenological gluon distribution of the latter set of partons.

## 5. Conclusions

We have studied the behaviour of the gluon distribution of the proton in the small  $x$  regime,  $10^{-4} < x < 10^{-3}$ , that has recently become accessible to the experiments being performed at the HERA electron-proton collider. In this regime it is necessary to work in terms of the unintegrated gluon distribution  $F(x; k_T^2)$  and to resum  $\ln(1=x)$  contributions. To leading order, the resummation is accomplished by the BFKL equation. The  $\sum_n \ln^n(1=x)$  contribution corresponds to an effective  $n$ -rung ladder diagram arising from a space-like chain of  $n$  gluon emissions. The solution  $F(x; k_T^2)$  of the BFKL equation shows, with decreasing  $x$ , two characteristic features. First an  $x$  growth (where  $\gamma = -\gamma_s 4 \ln 2$  for fixed  $s$ , or  $\gamma' = 0.5$  if  $s$  is allowed to run), and second, a diffusion or random walk in  $\ln k_T^2$  as we proceed along the gluon chain.

The full next-to-leading order summation of terms  $\sum_n \ln^{n-1}(1=x)$  is not yet known, but we would expect the description of  $F_2$  to be sensitive to this correction. However, two important higher-order effects can already be investigated. One effect is due to the angular ordering of gluon emissions, which leads to the CCFM, rather than the BFKL, equation for the gluon distribution. The solution now depends on an additional scale that is required to specify the maximum angle of gluon emission, which turns out to be essentially the scale  $Q^2$  of the probe. That the solution  $F(x; k_T^2; Q^2)$  will be dependent on  $Q^2$  is indeed evident from the angular ordering constraint  $(Q - qz)$  in the CCFM equation, (30). At very small  $x$  the constraint is automatically satisfied and the CCFM solution reduces to the BFKL form  $F(x; k_T^2)$ . Numerical solutions to the CCFM equation were obtained in ref. [11].

The second higher-order effect is due to the imposition of the kinematic constraint  $(k_T^2 = q_T^2 z)$  which is required for the validity of the BFKL or CCFM equation at small  $x$ . The constraint is needed to ensure that the virtuality of the gluons along the chain is controlled by the transverse momenta, that is  $j^2 \leq k_T^2$ . The major aim of this paper is to explore the consequences of implementing this constraint. For fixed  $s$  the introduction of the constraint preserves the scale invariance of the BFKL equation. The  $x$  behaviour of the solution as  $x \rightarrow 0$  can therefore be obtained using analytic methods. We found that the BFKL intercept  $\gamma = -\gamma_s 4 \ln 2$  is significantly reduced. The details are shown in Fig. 2. We see that it is insufficient to consider just next-to-leading effects; higher-order effects are important. For running  $s$  we solved the CCFM equation numerically and obtained the gluon distribution  $F(x; k_T^2; Q^2)$  with and without the kinematic constraint imposed. In this case the constraint has the effect of reducing  $\gamma$  by about 0.1, see Fig. 5. For  $Q^2 > k_T^2$  the kinematic constraint is more severe than that due to angular ordering and so the gluon distribution becomes independent of  $Q^2$ , see Fig. 4.

In Section 4 we studied the impact of imposing the kinematic constraint on the description of three observables which are sensitive to the gluon distribution at small  $x$  and which are

being measured at HERA. The observables are  $\sigma F_2 = \sigma \ln Q^2$ ,  $F_2^c(x; Q^2)$  and the  $W$  dependence of the cross section for high energy diffractive  $J = 0$  photoproduction. The effects are significant in particular regions of phase space; contrast the dashed and continuous curves in Figs. 7 and 9. As expected  $J = 0$  photoproduction offers an especially sensitive measure of the gluon. These comparisons with data should be regarded as exploratory, in other words, our calculation should be viewed as a preliminary step towards a full theoretical treatment of higher-order  $\ln(1/x)$  contributions. However, it is clear that the effects discussed in this paper should be incorporated in any realistic analysis of improved small  $x$  data.

## Acknowledgements

We thank Dick Roberts for valuable discussions. J.K. thanks the Department of Physics and Grey College of the University of Durham for their warm hospitality. This work has been supported in part by the UK Particle Physics and Astronomy Research Council, by Polish KBN Grant No. 2 P 03B 231 08 and the EU under Contracts Nos. CHRX-CT 92-0004 and CHRX-CT 93-0357.

## References

- [1] H1 collaboration: A. De Roeck et al., preliminary measurements to be published in the Proc. of the Workshop on DIS and QCD, Paris, 1995, DESY preprint 95{152.
- [2] ZEUS collaboration: M. Derrick et al., DESY preprint 95{193.
- [3] ZEUS collaboration: M. Derrick et al., Phys. Lett. B 350, 120 (1995);  
ZEUS and H1 collaborations; preliminary 1994 data presented at the Durham Workshop on HERA Physics, Sept. 1995, to be published.
- [4] S. Catani, M. Ciafaloni and F. Hautmann, Phys. Lett. B 242, 97 (1990); Nucl. Phys. B 366 657 (1991);  
J.C. Collins and R.K. Ellis, Nucl. Phys. B 360, 3 (1991);  
E.M. Levin, M.G. Ryskin and A.G. Shuvaev, Sov. J. Nucl. Phys. 53, 657 (1991).
- [5] M. Ciafaloni, Phys. Lett. B 356, 74 (1995).
- [6] E.A. Kuraev, L.N. Lipatov and V. Fadin, Zh. Eksp. Teor. Fiz. 72, 373 (1977) (Sov. Phys. JETP 45, 199 (1977));  
Ya. Ya. Balitzkij and L.N. Lipatov, Yad. Fiz. 28, 1597 (1978) (Sov. J. Nucl. Phys. 28, 822 (1978));  
L.N. Lipatov, in "Perturbative QCD", edited by A.H. Mueller, (World Scientific, Singapore, 1989), p. 441;  
J.B. Bronzan and R.L. Sugar, Phys. Rev. D 17, 585 (1978);  
T. Jaroszewicz, Acta. Phys. Polon. B 11, 965 (1980).

- [7] M. Ciafaloni, Nucl. Phys. B 296, 49 (1988).
- [8] B. Andersson, G. Gustafson and J. Samuelsson, Lund preprint LU TP 95-13.
- [9] J.R. Forshaw, P.N. Harriman and P.J. Sutton, Nucl. Phys. B 416, 739 (1994).
- [10] S. Catani, F. Fiorani and G. Marchesini, Phys. Lett. B 234, 339 (1990); Nucl. Phys. B 336, 18 (1990);  
G. Marchesini, in Proceedings of the Workshop "QCD at 200 TeV", Erice, Italy, 1990, edited by L. Cifarelli and Yu. L. Dokshitzer (Plenum Press, New York, 1992), p.183;  
G. Marchesini, Nucl. Phys. B 445, 49 (1995).
- [11] J. Kwiecinski, A.D. Martin and P.J. Sutton, Phys. Rev. D 52, 1445 (1995).
- [12] Yu. L. Dokshitzer, V. A. Khoze, S. I. Troyan and A. H. Mueller, Rev. Mod. Phys. 60, 373 (1988).
- [13] A. J. Askew, J. Kwiecinski, A.D. Martin and P.J. Sutton, Phys. Rev. D 47, 3775 (1993).
- [14] H1 collaboration : A. De Roeck, presented at the 2nd Krakow Epiphany Conference, January 1996, to be published in Acta Phys. Polon.
- [15] EM Collaboration : J.J. Aubert et al, Nucl. Phys. B 213, 31 (1983).
- [16] M. Glück, E. Reya and A. Vogt, Z. Phys. C 67, 433 (1995).
- [17] A.D. Martin, R.G. Roberts and W.J. Stirling, Phys. Lett. B 354, 155 (1995).
- [18] A. Vogt, DESY preprint DESY-96-012, hep-ph/9601352.
- [19] A.D. Martin, R.G. Roberts and W.J. Stirling, Phys. Rev. D 50, 6734 (1994).
- [20] J. Kwiecinski, A.D. Martin and P.J. Sutton, Durham preprint DTP/95/94, hep-ph/9511263.
- [21] M.G. Ryskin, Z. Phys. C 57, 89 (1993).
- [22] S. Brodsky et al, Phys. Rev. D 50, 3134 (1994).
- [23] M.G. Ryskin, R.G. Roberts, A.D. Martin and E.M. Levin, University of Durham report DTP/95/96.

## Figure Captions

Fig.1 Gluon emission which forms the basis of the BFKL equation (1) for the unintegrated gluon distribution  $F(x; k_T^2)$ .  $x$  and  $x=z$  are the longitudinal momentum fractions of the proton's momentum carried by the respective gluons. Throughout we use  $q_T$  and  $k_T$  to denote, respectively, the transverse momentum of an emitted gluon and of a gluon along the chain.

Fig.2 The exponent of the  $x$  behaviour of the gluon distribution obtained by solving the BFKL equation (a) with (continuous curve) and (b) without (dashed curve) the kinematic constraint imposed, as a function of (fixed)  $\bar{\alpha}_s = 3$ . The dashed curve is  $\bar{\alpha}_s = 4 \ln 2$ . The dotted curve (c) is the value of the exponent that is obtained if we keep only the next-to-leading order modification due to the kinematic constraint.

Fig.3 The continuous curves are the effective exponent  $\epsilon = \partial \ln F / \partial \ln(1/x)$  calculated from the numerical solution  $F(x; k_T^2)$  of the BFKL equation which incorporates the kinematic constraint, for  $k_T^2 = 1000, 100, 10$  and  $4 \text{ GeV}^2$ . The coupling  $\bar{\alpha}_s = 3$ ,  $\bar{\alpha}_s = 0.2$ . The dashed lines indicate the value of the exponent of the  $x \rightarrow 0$  analytic solutions of the BFKL equation with and without the kinematic constraint included, that is the values of curves (b) and (a) of Fig.2 respectively at  $\bar{\alpha}_s = 0.2$ .

Fig.4 The  $Q^2$  dependence of the gluon distribution  $F(x; k_T^2; Q^2)$  obtained by solving the CCFM equation with (continuous curves) and without (dashed curves) the kinematic constraint (33) included. Results are shown for  $x = 10^{-5}; 10^{-4}; 10^{-3}$  and  $10^{-2}$ .

Fig.5 The effective exponent  $\epsilon = \partial \ln(xg) / \partial \ln(1/x)$  obtained by solving the CCFM equation with (continuous curves) and without (dashed curves) the kinematic constraint (33) included. Results are shown for  $Q^2 = 1000; 100; 10$  and  $4 \text{ GeV}^2$ .

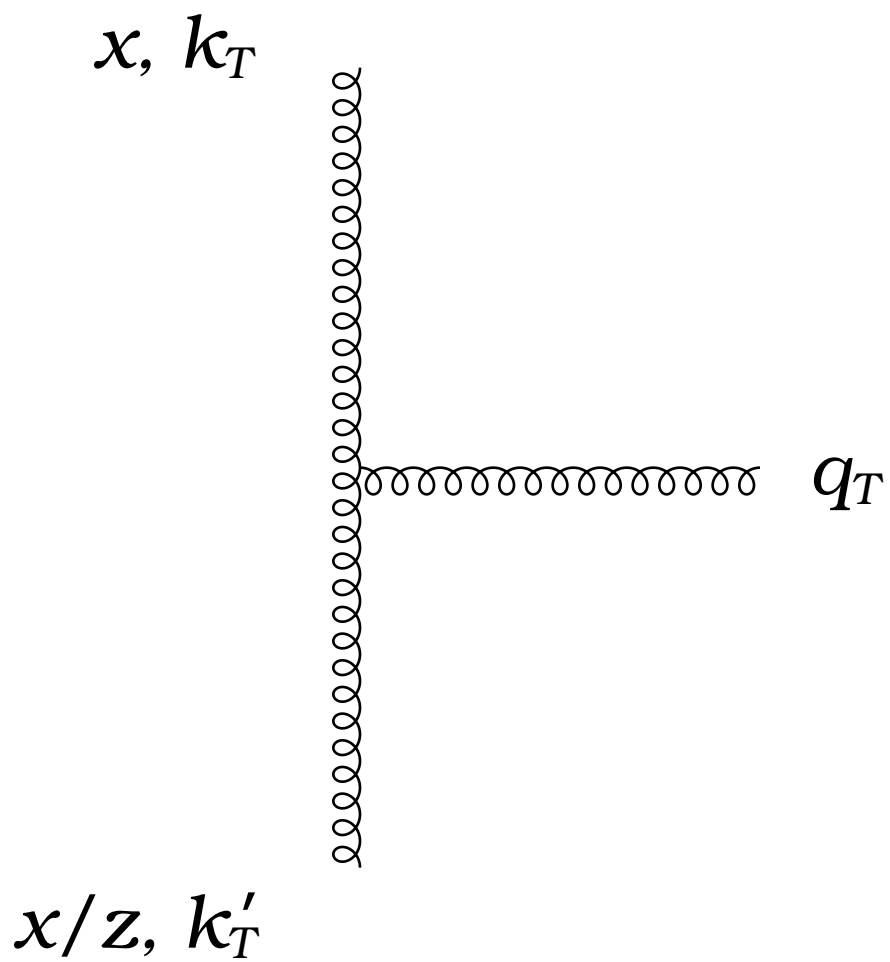
Fig.6 Pictorial representation of the  $k_T$  factorization formula, that is of the convolution  $F_2 = \int_q^P F_q F_q^{\text{box}}$  of (40).  $F(x^0; k_T^2; Q^2)$  is the unintegrated gluon distribution and  $\int_q^P F_q^{\text{box}}$  is the off-shell gluon structure function, which at lowest order is determined by the quark box (and "crossed box") contributions.

Fig.7 Predictions of the proton structure function  $F_2(x; Q^2)$  as a function of  $\ln Q^2$ , at fixed values of  $x$ , compared with recent measurements made by the experiments at HERA [1, 2]. The continuous and dashed curves are respectively the predictions obtained from the CCFM equation, via the  $k_T$ -factorization theorem, with and without the kinematic constraint (33) incorporated. The dotted curves are the predictions obtained from the GRV set of partons [16].

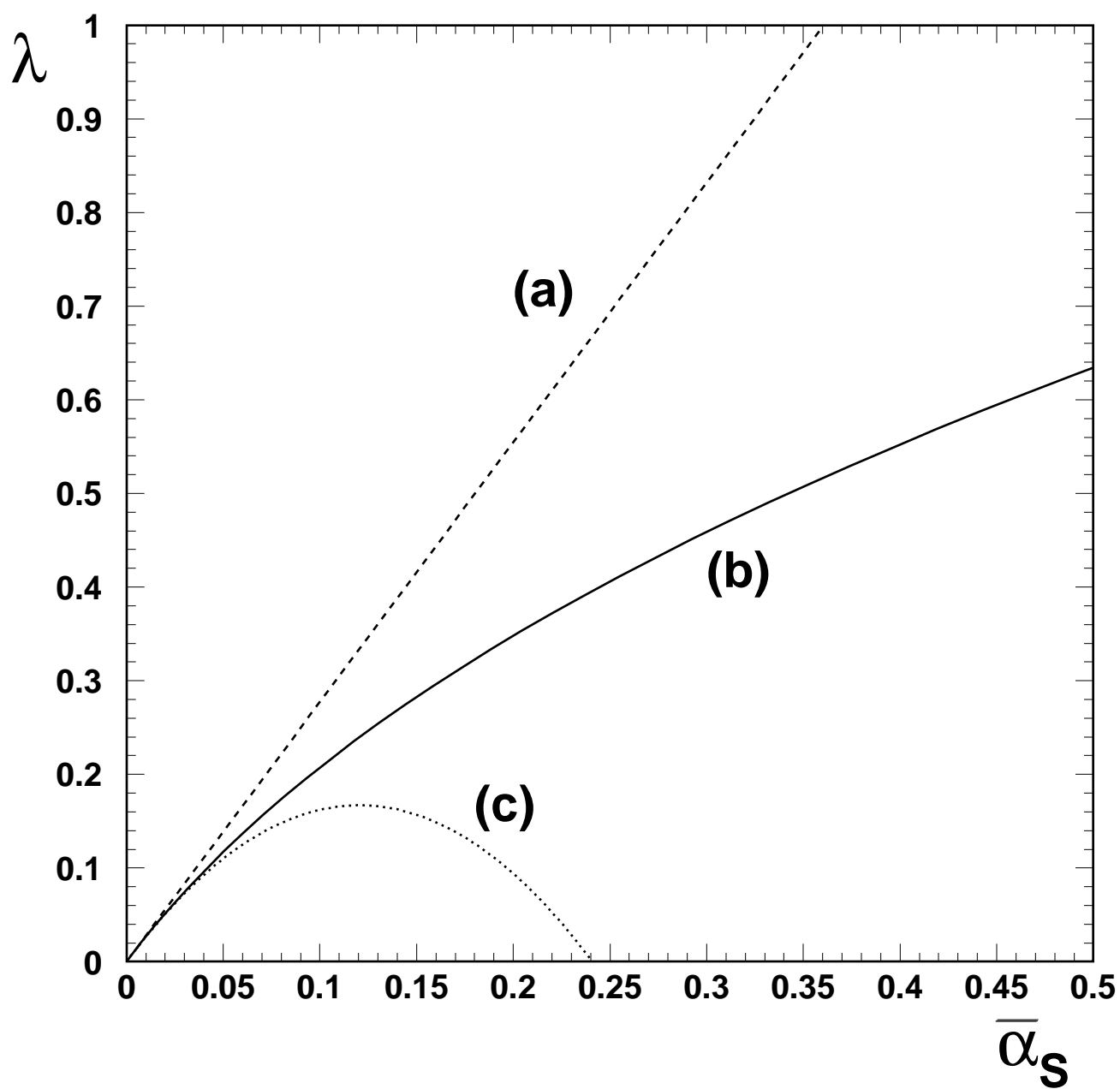
Fig.8 Predictions for the charm component  $F_2^c$  of the proton structure function,  $F_2$ , compared to recent preliminary H1 measurements [14] and older EMC data [15]. The predictions were obtained by solving the CCFM equation (with kinematic constraint) for the unintegrated

gluon and then using the  $k_T$ -factorization formula with  $m_c = 1.4 \text{ GeV}$  (upper continuous curve) and  $m_c = 1.7 \text{ GeV}$  (lower continuous curve). Also shown are the next-to-leading order predictions [18, 19] based on GRV [16] and MRS [17] partons.

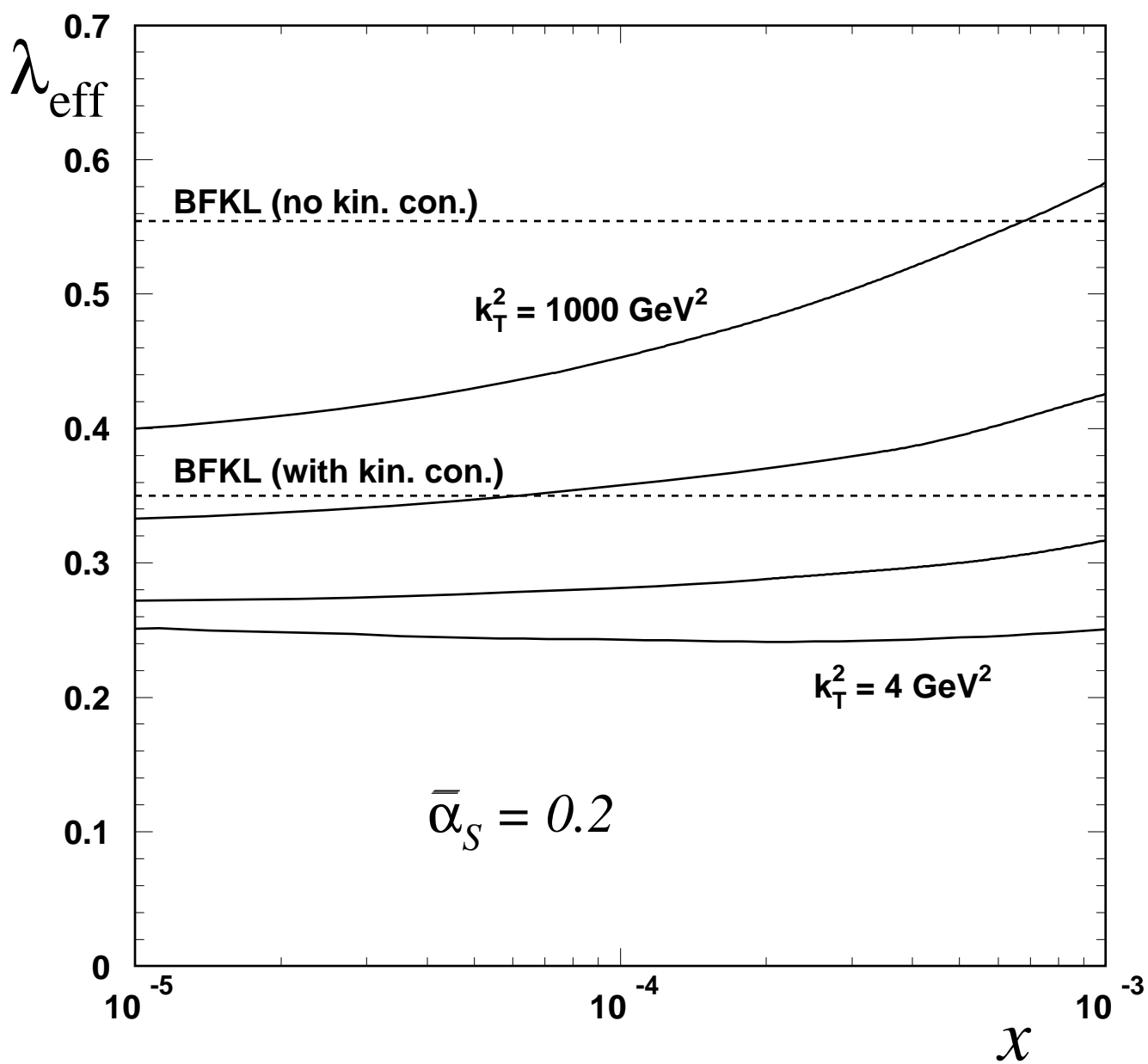
Fig. 9 The measurements [3] of the cross section for diffractive  $J/\psi$  photoproduction compared with the perturbative QCD description based on the unintegrated gluon distribution obtained by solving the CCFM equation with (continuous curve) and without (dashed curve) the kinematic constraint (33) included. The dotted and dash-dotted curves are the predictions obtained from the GRV and MRS ( $A^0$ ) set of partons [16, 17], calculated as in ref. [23].



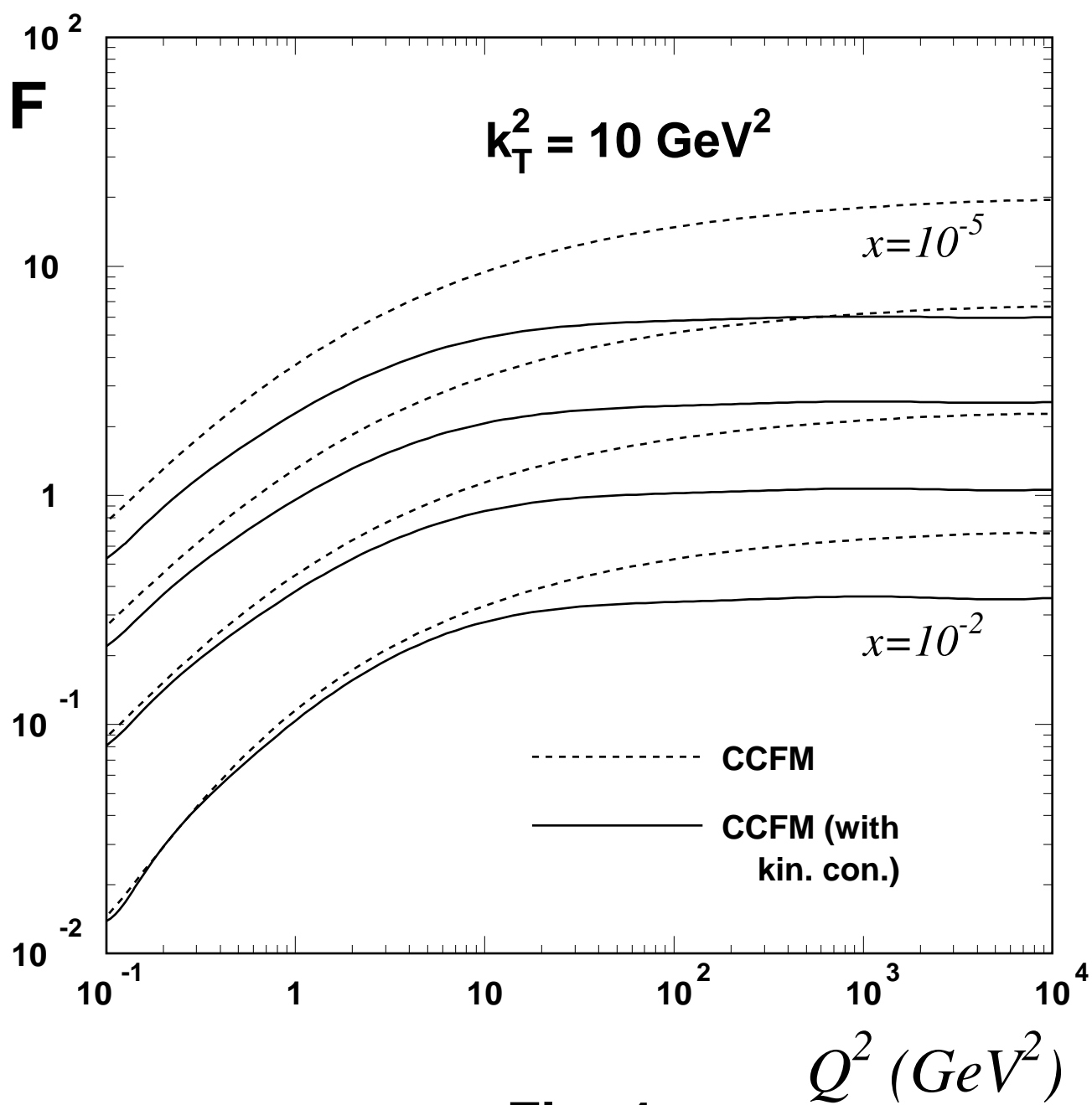
**Fig. 1**



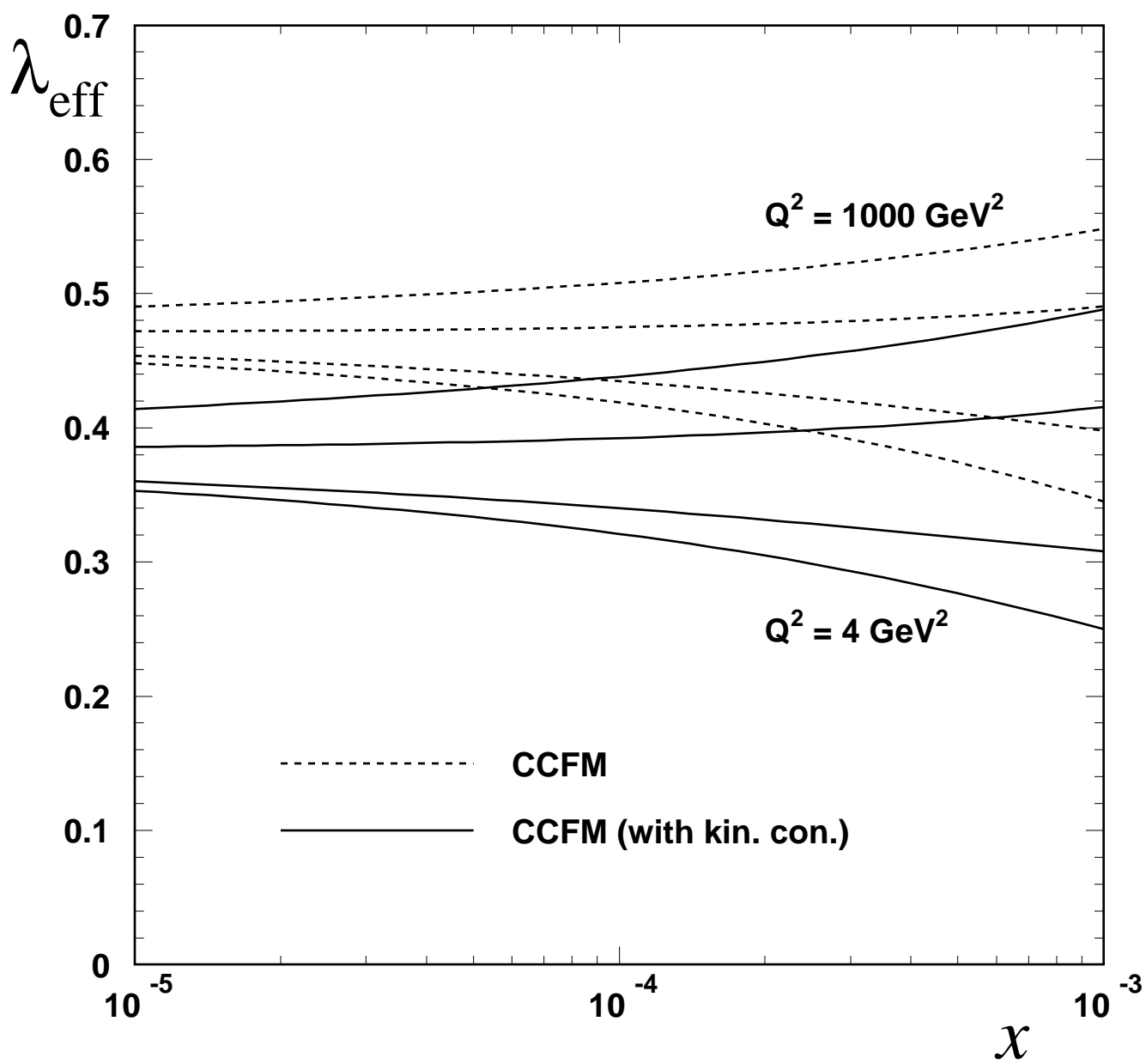
**Fig. 2**



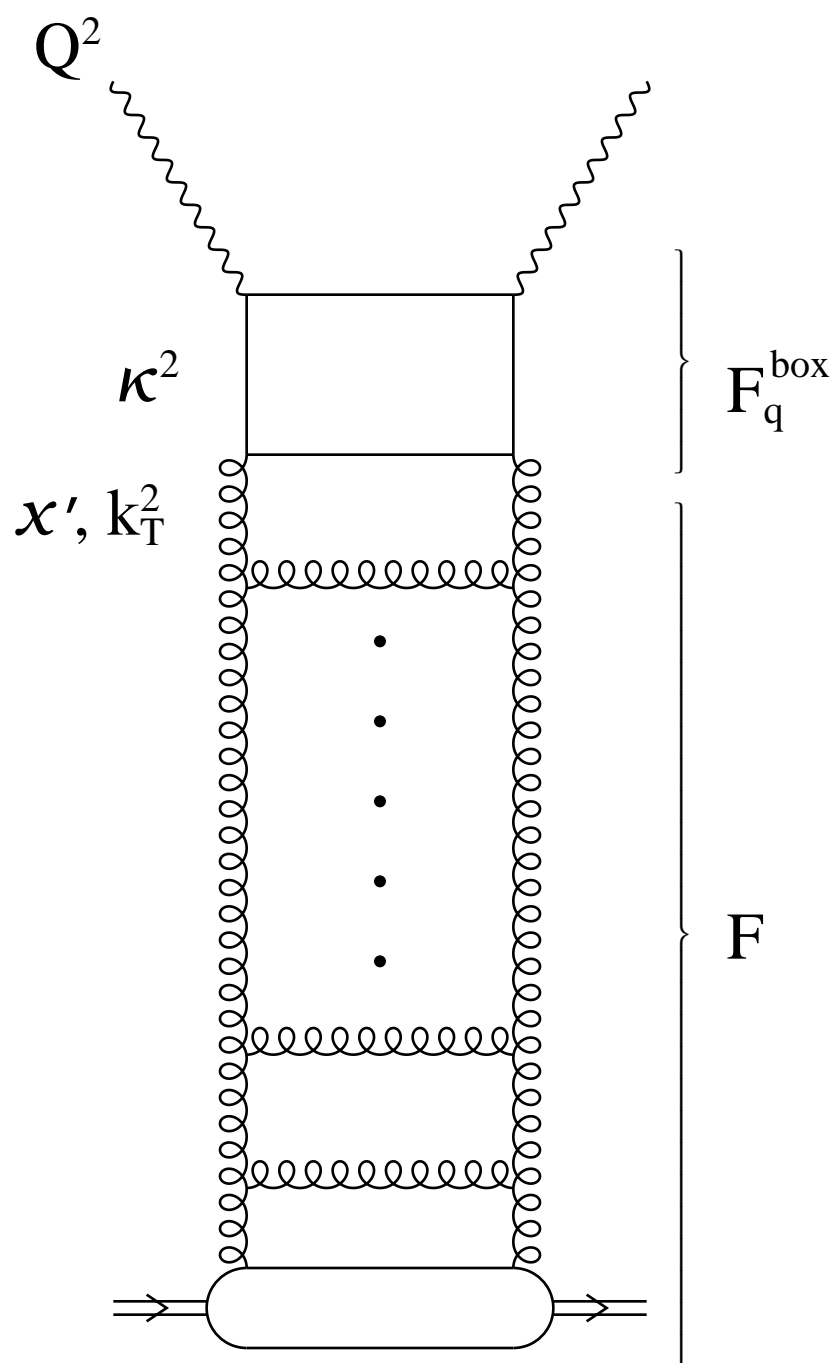
**Fig. 3**



**Fig. 4**

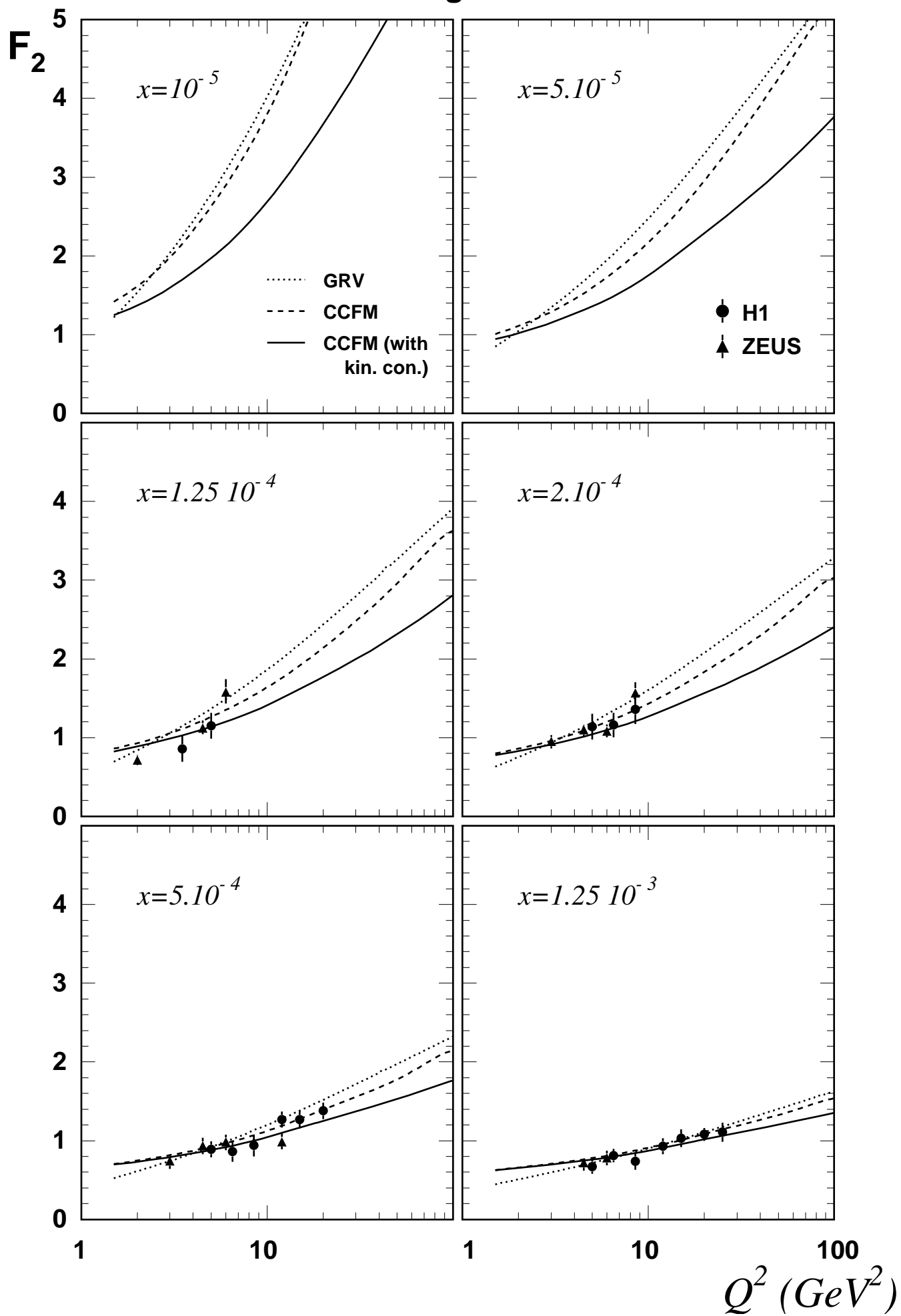


**Fig. 5**

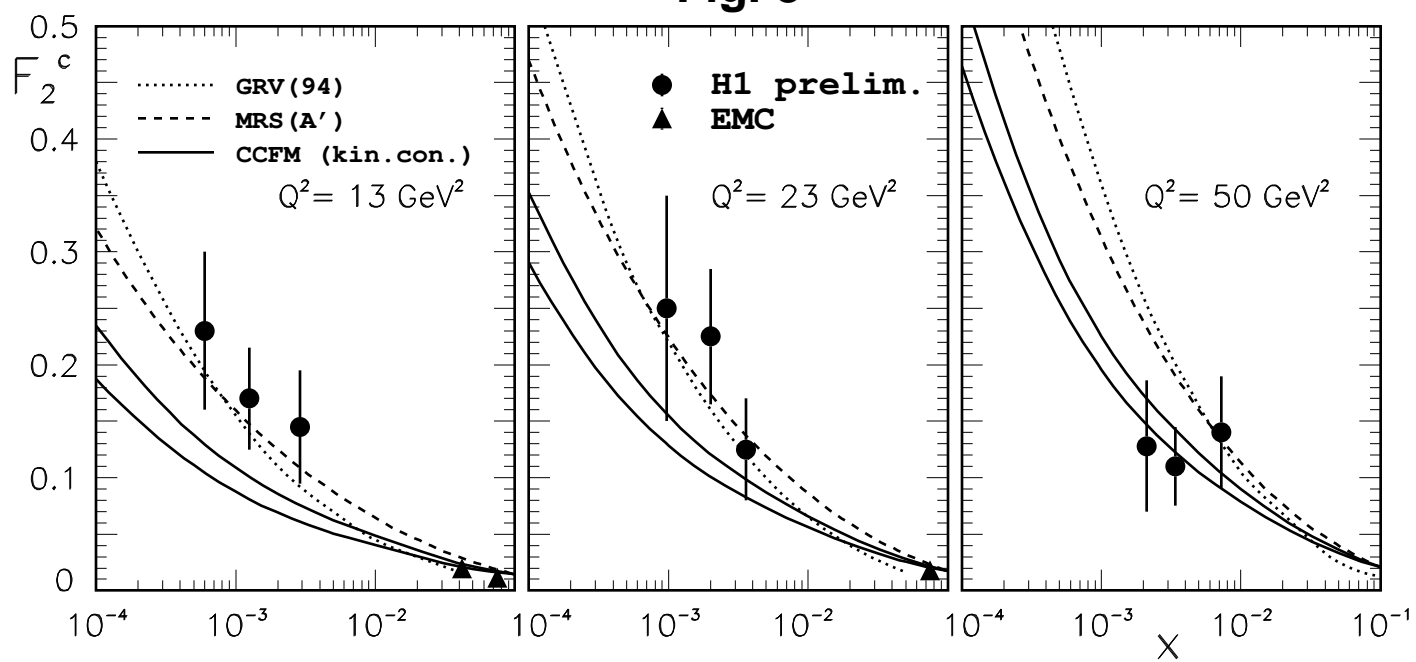


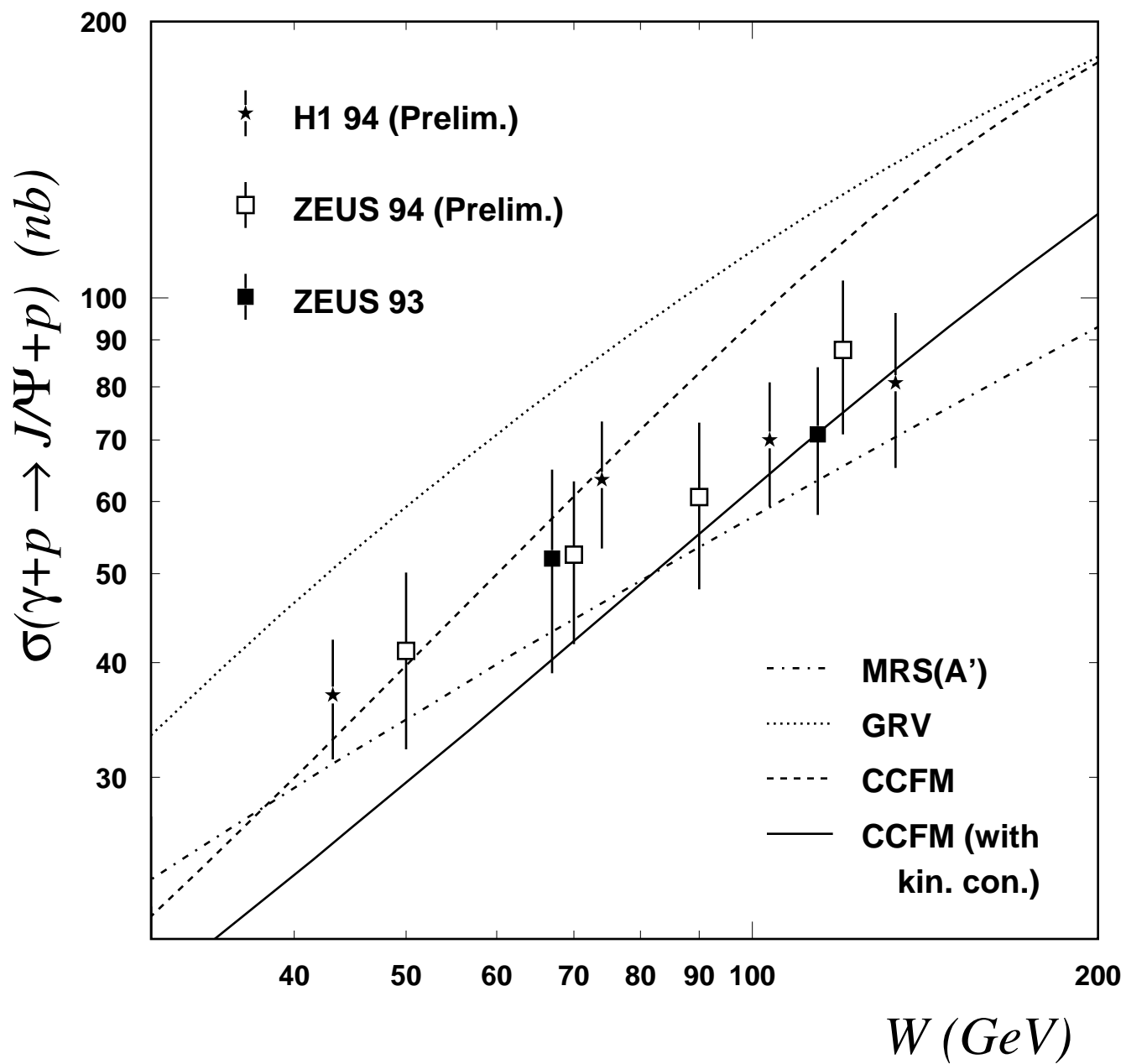
**Fig. 6**

Fig. 7



**Fig. 8**





**Fig. 9**